AIP | APL Materials

Tuning cationic composition of La:EuTiO3 films

Andrey Shkabko, Chencheng Xu, Paul Meuffels, Felix Gunkel, Regina Dittmann, Anke Weidenkaff, and Rainer Waser

Citation: APL Materials **1**, 052111 (2013); doi: 10.1063/1.4831856
View online: http://dx.doi.org/10.1063/1.4831856
View Table of Contents: http://scitation.aip.org/content/aip/journal/aplmater/1/5?ver=pdfcov
Published by the AIP Publishing

Tuning cationic composition of La:$EuTiO_{3-\delta}$ films

Andrey Shkabko,[1,2,a] Chencheng Xu,[1] Paul Meuffels,[1] Felix Gunkel,[1] Regina Dittmann,[1] Anke Weidenkaff,[2] and Rainer Waser[1]
[1]*Forschungszentrum Jülich, Peter Grünberg Institut (PGI-7), D-52425 Jülich, Germany*
[2]*Empa, Solid State Chemistry & Catalysis, CH-8600 Dübendorf, Switzerland*

(Received 2 September 2013; accepted 5 November 2013; published online 26 November 2013)

$Eu_{1-x}La_xTiO_{3-\delta}$ (x = 0, 0.3, 0.5) films were deposited in a p(Ar(96%)/H_2(4%)) $= 4 \times 10^{-4}$ mbar atmosphere on $(LaAlO_3)_{0.3}$-$(Sr_2AlTaO_6)_{0.7}$ vicinal substrates (0.1°). Reflection high-energy electron diffraction oscillation characteristics of a layer-by-layer growth mode were observed for stoichiometric and Ti-rich films and the laser fluence suited to deposit stoichiometric films was identified to be 1.25 J/cm^2 independent of the La content. The variety of resulting film compositions follows the general trend of Eu-enrichment for low laser and Ti-enrichment for high laser fluence. X-ray diffraction confirms that all the films are compressively strained with a general trend of an increase of c-axis elongation for non-stoichiometric films. The surfaces of non-stoichiometric films have an increased roughness, the highest sheet resistances, exhibit the presence of islands, and are Eu^{3+} rich for films deposited at low laser fluence. [http://dx.doi.org/10.1063/1.4831856]

Transition metal perovskite oxides ABO_3 show a variety of properties which highly depend on the oxygen as well as on the cation content. The wide band-gap insulator (3.2 eV) $SrTiO_3$ (STO) and the smaller band-gap black-colored insulator (1 eV) $EuTiO_3$ (ETO) show, for example, metal-to-insulator transitions, anomalous Hall behavior[1] and high thermopower[2,3] when slightly doped on cationic sites or with oxygen vacancies. These properties are highly bound to the growth control of films[3]/single crystals with variable doping concentrations and stoichiometry control for metal-to-insulator transitions arising through valence change and/or band-gap closure[4] mechanisms.

STO is known for its high electron mobility[5] with a potential for future oxide electronics and the control of the stoichiometry in ultrathin films is an important factor. Thus, recent advances in pulsed laser deposition (PLD) and molecular beam epitaxy techniques resulted in extended investigations especially with respect to the impact of oxygen partial pressure $p(O_2)$,[6] laser fluence,[7,8] etc., on the electric transport of the STO films and interfaces. ETO is another candidate for oxide electronics being isostructural to STO and additionally to its structure similarities, very peculiar electromagnetic coupling properties have been the topic of recent years.

In $EuTiO_3$ the knowledge about sample preparation parameters and stoichiometry is crucial for realization of magnetocoupling in the material, as local symmetry breaks creating ferroelectric domains.[9–11] Not only doping[1] and disorder, but also strain[12] in case of thin films can induce the shift of the ferroelectric transition temperature from 5 K up to 250 K[13] in 22 nm ETO thick films grown on $DyScO_3$ [110] and induce ferromagnetism.[14] Additionally, the stress induced by nanostructuration in the nanowires is predicted to induce ferroelectricity in ETO.[15]

Since ETO is isostructural to $Sr^{2+}Ti^{4+}O_3^{2-}$ with identical ionic charges Eu^{2+}, Ti^{4+}, O^{2-} filling the perovskite,[16] it can induce interface conductivity, e.g., like in $SrTiO_3/LaAlO_3$, due to similar electrostatic potential/strain which can be created at between $EuTiO_3$ and $LaAlO_3$. Similar

[a]shkabko@gmail.com

TABLE I. List of prepared films. PLD parameters/settings for the deposition of undoped and La-doped ETO thin films on LSAT[001] substrates under a background pressure of $p(\mathrm{Ar}\ (96\%)/\mathrm{H_2}(4\%)) = 4 \times 10^{-4}$ mbar and at a temperature of $T_S = 1073$ K (u.c.: unit cell), resistivities, Hall mobilities, and carrier concentrations at 300 K.

Target	Laser fluence (J/cm^2)	Laser repetition rate (Hz)	Pulses (u.c.)	Thickness (~u.c.)	Resistivity (300 K) (Ω cm)	Hall mobility, μ_H (300 K) (cm^2/V s)	Carrier concentrations, n (300 K) ($\times 10^{19}$ cm^{-3})
$EuTiO_{3-\delta}$	0.8	2	~200	10	0.5	0.38	3.28
$EuTiO_{3-\delta}$	1.25	2	80	20	1	0.22	2.7
$EuTiO_{3-\delta}$	2	1	29	20	1	0.33	1.84
$E_{0.97}La_{0.03}TiO_{3-\delta}$	0.8	2	~200	10	4.72	...	...
$E_{0.97}La_{0.03}TiO_{3-\delta}$	1.25	2	68	20	0.1	1.57	3.9
$E_{0.97}La_{0.03}TiO_{3-\delta}$	2	1	30	20	0.26	0.65	3.67
$E_{0.95}La_{0.05}TiO_{3-\delta}$	0.8	2	~200	10	1.33	...	...
$E_{0.95}La_{0.05}TiO_{3-\delta}$	1.25	2	71	20	0.08	1.67	4.79
$E_{0.95}La_{0.05}TiO_{3-\delta}$	2	1	33	20	0.12	1	5

to $SrTiO_3/LaAlO_3$ it can be realized by either (i) positively charged oxygen vacancies in $EuTiO_3$ creating electron conduction, or (ii) by depositing alternating polar $(LaO)^+$ and $(AlO_2)^-$ layers on top of $(TiO_2)^0$ terminated ETO. Thus, investigations of ultrathin films where the strain is either due to chemical doping(La^{3+})/cation non-stoichiometry/oxygen vacancies[17] and imposed by substrate-film interactions are of importance to create conducting interfaces.

In this work the first investigations of the growth and electrical properties measurements of undoped and A-site (ABO_3) electronically doped La^{3+} ETO in Ar/H_2 atmospheres are presented. Similar to known conducting $La_xSr_{1-x}TiO_3$,[18] La^{3+} doping in ETO transforms the perovskite into more conducting one. We reveal deposition scenarios for the growth of disordered films which are independent of rather small La chemical doping. These scenarios are very similar to the STO grown in O_2 as a background atmosphere as a function of laser fluence.

Undoped and La (3, 5 at.%)-doped ETO thin films were deposited on $(LaAlO_3)_{0.3}$-$(Sr_2AlTaO_6)_{0.7}$ (LSAT) [001] substrates by means of PLD. The ceramic targets used for PLD were synthesized by solid-state reactions of Eu_2O_3 (99.9% purity, Sigma-Aldrich; dried before weighing), TiO_2 (99.9+%, Sigma-Aldrich), and La_2O_3 (99.99%, Alfa Aesar; dried before weighing) powders. Appropriate amounts of the reactants were thoroughly mixed together using a ball mill. The powder mixtures were then calcined two times – with intermediate grinding – at 1000 °C for 24 h under a flowing gas of $Ar(96\%)/H_2(4\%)$. In this way, single-phase materials were synthesized as could be shown by X-ray diffraction. Afterwards, the resulting materials were ground again, pressed into pellets and sintered at 1400 °C for 8 h in $Ar(96\%)/H_2(4\%)$ to obtain high-density targets.

Following established high temperature annealing procedures in order to create TiO_2 terminated LSAT,[19,20] the as received LSAT substrates (Crystec GmbH) with a vicinal angle of 0.1° were annealed at 950 °C for 4 h in air and cooled down in a natural way prior to deposition in order to create a regular terrace structure with a typical terrace width of 200 nm. A KrF excimer laser was used to ablate the targets in order to grow a series of thin films using the parameters/settings that are listed Table I. The film growth was monitored by reflection high-energy electron diffraction (RHEED) measurements. After growth, the films were quenched by switching off the laser heater to room temperature in deposition atmosphere.

X-ray photoelectron spectroscopy (XPS) analysis was performed with a PHI 5000 Versa Probe using monochromatic Al-K_α radiation. To determine the composition of the ETO thin films, the Eu 4*d*, Ti 2*p*, and O 1*s* spectral lines were recorded and the collected data were evaluated using the PHI MultiPak 9.3 software. The electron take-off angle was set to 45° and the analyzer was operated in the constant pass energy mode for all measurements. The analyzer pass energy was set to 46.95 eV with a step size of 0.2 eV. The C 1*s* signal position at a binding energy of 284.8 eV was used for reference. Atomic force microscopy was applied in the tapping mode to investigate the

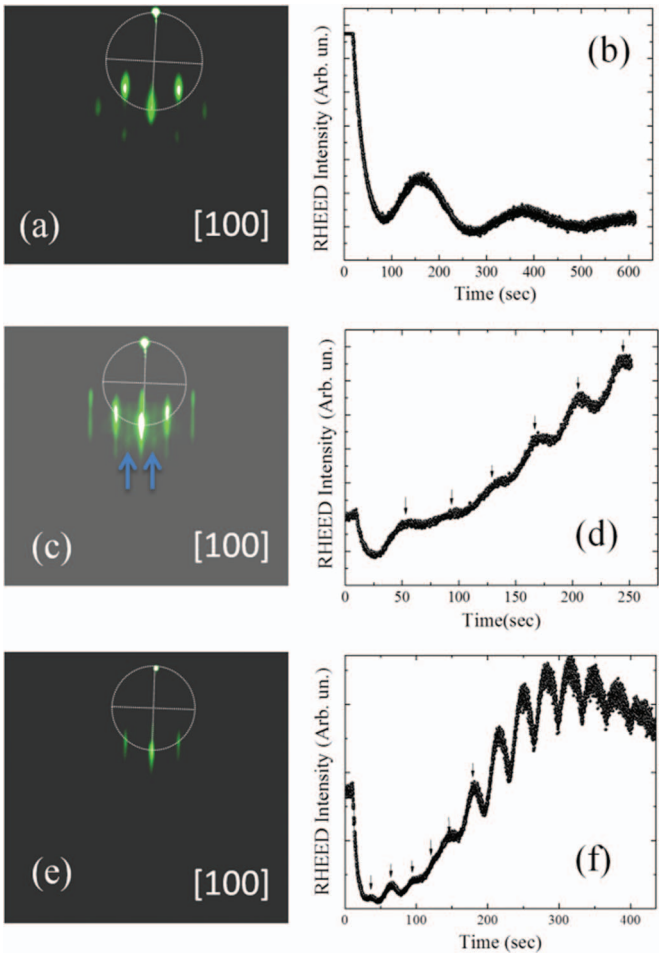

FIG. 1. Typical final RHEED patterns along [100] azimuth (Laue circle is depicted in white) (a), (c), and (e) and RHEED intensity of the specular spot (b), (d), and (f) for 0.8 J/cm^2 (Eu-rich), 1.25 J/cm^2 (stoichiometric), and 2 J/cm^2 (Ti-rich) films. Blue arrows (c) show 1/2 order surface reconstruction.

surface morphology of the substrates and films. The sheet resistances (300 K) and Hall mobilities (300 K) were measured using van der Pauw technique on Physical Properties Measurement System (PPMS) QD.

Annealed LSAT vicinal substrates (0.1°) exhibit the typical reciprocal space RHEED pattern (not shown) as observed for smooth surfaces of the cubic perovskite STO with characteristic spots being located on the Laue circle. Fig. 1(a) represents the typical final RHEED pattern along the [100] azimuth for films deposited at 0.8 J/cm^2 laser fluence with characteristic cubic pattern corresponding to reciprocal space of 3D- cubic perovskite structure indicating a 3D growth mode. The intensity of the specular spot, Fig. 1(b), shows oscillations which in the best cases damp out after the deposition of roughly two unit cells (normally, no oscillations are observed) indicating a final 3D growth mode.

Fig. 1(c) represents the typical RHEED pattern along the [100] azimuth for films deposited at a laser fluence of 1.25 J/cm^2 which was acquired at the end of deposition. The pattern shows the same characteristic as that of the surface of as prepared LSAT substrates with present 1/2 order reconstruction indicated by blue arrows as found on $SrTiO_3$.[21] The RHEED intensity of the specular spot, Fig. 1(d), shows characteristic oscillations and a magnitude increase indicating a 2D layer-by-layer growth mode.

Fig. 1(e) represents the typical RHEED pattern along the [100] azimuth for films deposited at 2 J/cm^2 laser fluence which was acquired at the end of deposition. The pattern corresponds to the RHEED pattern of the surface of as prepared LSAT substrates. The intensity oscillations of

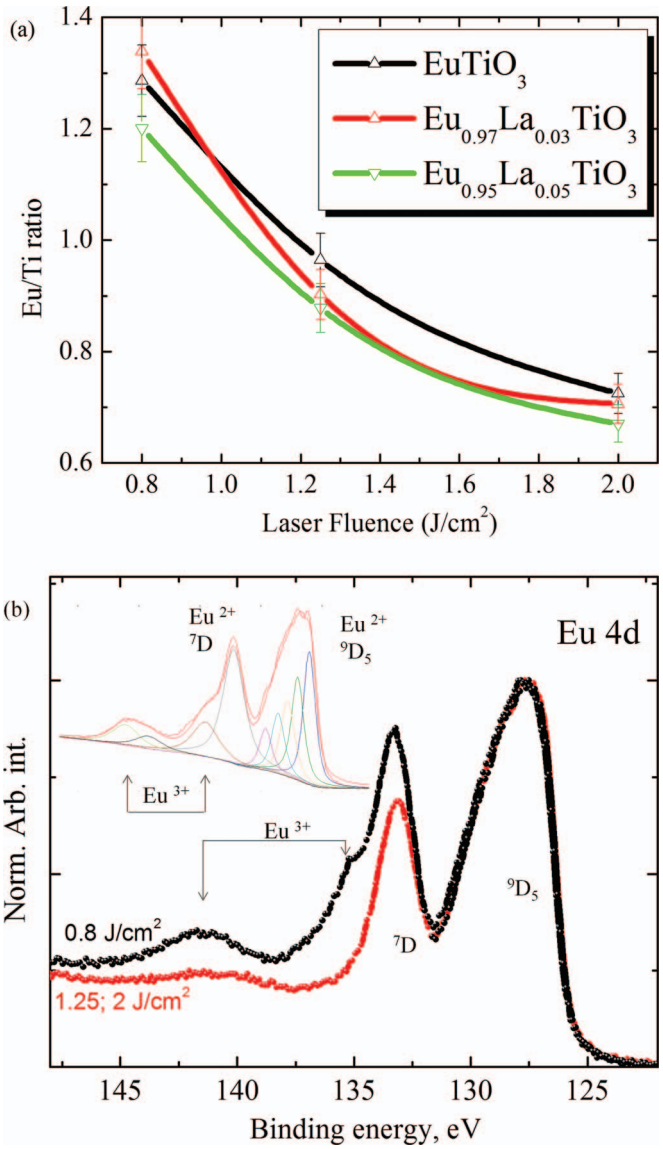

FIG. 2. (a) Cation ratio Eu/Ti of the deposited films as a function of laser fluence as evaluated from XPS measurements; the lines are guides for the eye. (b) Typical Eu 4*d* XPS spectra for ETO films deposited using a laser fluence of 0.8 J/cm^2 (black) and 1.25 and 2 J/cm^2 (red).

the specular spot, Fig. 1(f), show characteristic oscillations and a magnitude increase confirming layer-by-layer growth mode. However, time between the peaks changes its periodicity corresponding to "unstable" growth due to stoichiometry variations as will be shown later in the text.

We have to stress that independently of the La content of the ETO films, the deposition at low laser fluences was ruled by a 3D growth mode of the cubic-type perovskite resulting in films with rough surfaces. However, at higher laser fluences a 2D layer-by-layer growth mode was established with characteristic oscillations corresponding to 1 unit cell of the perovskite structure, see Figs. 1(d) and 1(f).

Photoelectron spectroscopy was used to determine the film composition and the chemical state of the constituting elements. Fig. 2(a) represents the cation concentration ratio Eu/Ti of as-prepared films as a function of the laser fluence during deposition. As a reference for the ratio Eu/Ti = 1, additional XPS measurements were performed on the cleaved surface of a ETO single crystal. From the results it can be concluded that Eu-rich films are formed when a low laser fluence is used during

the deposition whereas Ti-rich films are formed at high laser fluences. Similar dependencies of the cation ratio Sr/Ti on laser fluence were found for STO thin films deposited by means of PLD.[19,22]

Fig. 2(b) represents the Eu 4*d* XPS spectra measured on films deposited at a laser fluence of 0.8 J/cm^2 and 1.25 J/cm^2. The spectra measured on films deposited at a laser fluence of 1.25 J/cm^2 and 2 J/cm^2 exhibit no essential differences in shape, shift, and relative intensities as indicated in red. The Eu 4*d* multiplet structure is complex and not only consists of pair of $4d_{5/2}$ and $4d_{3/2}$ spin-orbit peaks due to the strong 4*d*-4*f* exchange interaction and a weaker spin-orbit splitting of the 4*d* orbitals.[23] The main peaks are centered at about $E_b = 127.8$ eV and $E_b = 133.6$ eV resulting from Eu^{2+} and are assigned to ^{7}D and ^{9}D multiplets,[23] respectively, confirming Eu^{2+} as most chemical state present in the films deposited at 1.25 J/cm^2 and 2 J/cm^2. The fine structure of the ^{9}D peak was fitted with five peak-components according to the electron spectroscopic theories for rare-earths elements as described in Ref. 24 (see inset in Fig. 2(b)). The Eu^{3+} doublet slightly present in the 0.8 J/cm^2 deposited films is shifted by about 7 eV away from the Eu^{2+} doublet[25] towards higher binding energies and has a higher intensity for Eu-rich films. The observable difference of the Eu-rich samples as compared to stoichiometric and Ti-rich is the presence of Eu^{3+} which is most probably due to the formation of Eu_2O_3 on the film surface after the excess of EuO was exposed to air. Indeed, unprotected EuO is known to rapidly oxidize in air if prepared without a protecting capping layer, thus resulting in an extra amount of Eu^{3+}.[23] Taking into account that XPS Ti 2*p* spectra (not shown) correspond to Ti^{4+} state without exceptions for all the samples and electron charge balance affects only Eu ions, the first probable scenario for secondary phase $Eu_2^{3+}O_3^{2-}$ formation can be written as follows:

$$Eu_{1+x}^{2+}Ti^{4+}O_{3+x}^{2-} + \left(\frac{x}{2}\right)O_2 \rightarrow Eu^{2+}Ti^{4+}O_3^{2-} + (x/2)Eu_2^{3+}O_3^{2-},$$

where the first summand of the left side corresponds to the uncompensated as-deposited film which is exposed to O_2 (second summand) and the second summand of the right side corresponds to a secondary phase which forms due to charge compensation mechanism.

A second possible scenario for the Eu^{3+}-enrichment can be the accommodation of Ti vacancies in the perovskite structure. Assuming Ti vacancies formation in ETO as a similar process during the growth of Sr-rich $SrTiO_3$ at low laser fluencies,[26] Ti vacancies have to be compensated by Eu ions in higher oxidation state like Eu^{3+}.

Fig. 3(a) represents the typical surface morphology of films deposited at 0.8 J/cm^2 laser fluence. A terrace structure can hardly be discerned and rod-like nanocrystallites are present with length up to 500 nm and height of 5–6 nm. From the XPS data these nanorods possibly consist of Eu_2O_3 containing phases nominally having an excess of Eu^{3+}. Fig. 3(b) represents the typical surface morphology of films deposited at 1.25 J/cm^2. The surface shows terraces corresponding to the vicinal angle of the substrate with steps of heights 1–2 ETO unit cells (0.39 nm). Fig. 3(c) represents the typical surface morphology of films deposited at 2 J/cm^2. The surface exhibits round shaped islands with diameters of about 50 nm and heights of about a 1–1.5 nm. These islands are probably TiO_2 precipitations which – as known from some studies on STO films – grow in a round shaped manner.[27]

Fig. 4(a) shows XRD ($\theta - 2\theta$) scans around the LSAT [002] diffraction peak revealing phase-pure epitaxial [001]-oriented $EuTiO_{3-\delta}$ films with characteristic Kiessig fringes.[28] Similar diffraction patterns are obtained for La-doped ETO films with the weaker thickness fringes only for thinner (10 u.c.) films deposited at 0.8 J/cm^2. The presence of the fringes indicates that all films have good crystallinity despite the fact of 3D growth for Eu-rich films. The film thicknesses calculated from the distance between the Kiessig fringes are presented in Table I and are in agreement with those estimated from the RHEED oscillations of the specular spot, Fig. 1. The out-of-plane lattice parameters for all the films are presented in Fig. 4(b). It can be seen that Eu- and Ti-rich films show an increase of the out-of-plane lattice constant. This feature reminds of similar findings on Sr- and Ti-rich STO films.[29]

All the deposited films exhibit electrical charge transport with a resistivity of 1 Ω cm for nominally stoichiometric film of $EuTiO_{3-\delta}$ which is in agreement with Takahashi,[1] however our La-doped stoichiometric films are of bit higher resistivity than reported. Eu-rich films have systematically

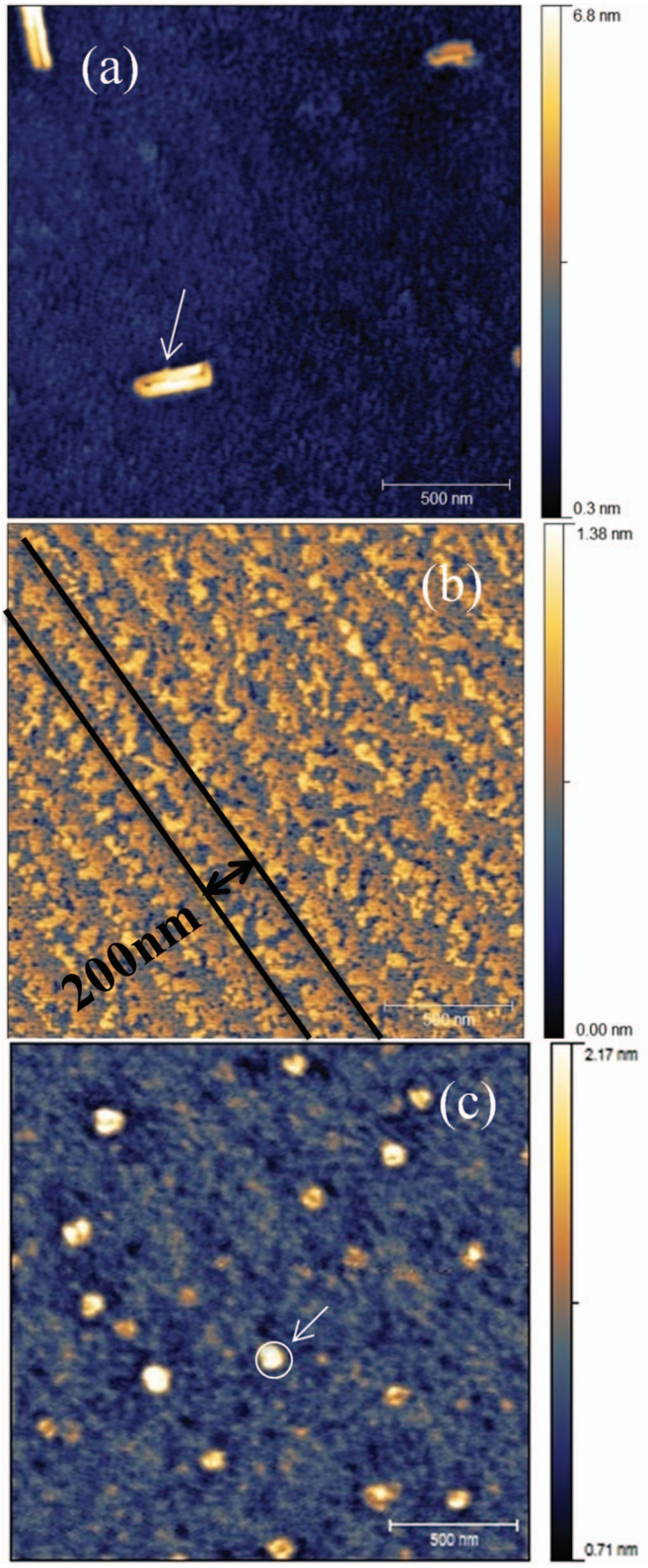

FIG. 3. Typical atomic force microscopy (AFM) topography images for low laser fluence 0.8 J/cm^2 (Eu-rich), middle fluence 1.25 J/cm^2 (stoichiometric), and high fluence 2 J/cm^2 (Ti-rich). The arrows in (a) and (c) show specific features which are most probably Eu_2O_3 and TiO_2 precipitates, respectively.

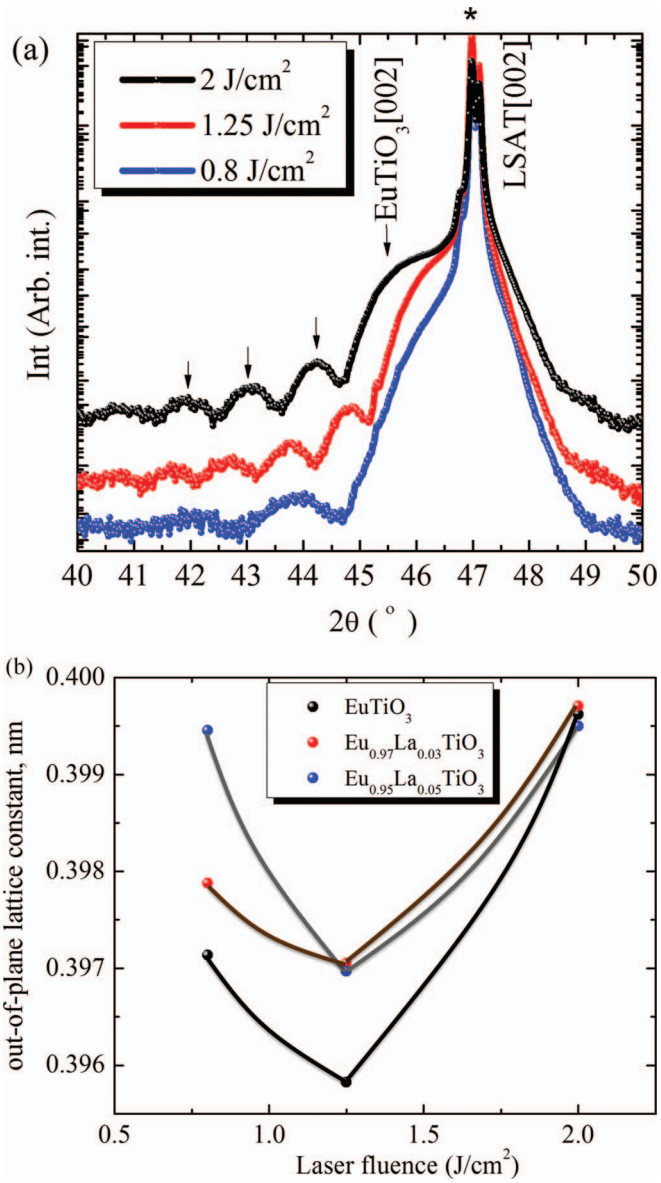

FIG. 4. (a) XRD ($\theta - 2\theta$) scans around the LSAT [002] peak ($K_{\alpha 1}/K_{\alpha 2}$), $K_{\alpha 1}$ ($2\theta = 46.985$ LSAT [002] marked by asterisk) with thickness oscillations (shown by arrows) corresponding to the $EuTiO_{3-\delta}$ films. (b) Out-of-plane (a = b) lattice constant as a function of laser fluence for as deposited films (lines are guides for the eye).

higher resistivity than stoichiometric and Ti-rich films with the only exception for nominally undoped ETO films, when resistivity of Eu-rich film is twice lower than doped and Ti-rich films. The carrier concentrations of electrons in the films are all in the range of (2–5) $\times$ 10^{19} cm^{-3} with 2.7 $\times$ 10^{19} cm^{-3} for $EuTiO_{3-\delta}$ confirming that electrical conductivity is most probably determined by partial oxygen pressure during the growth and thus induced oxygen vacancies. Considering the amount of oxygen vacancies and amount of their induced electrons constant for stoichiometric films, the carrier concentrations of 5% and 3% doped stoichiometric films should give 1.66 ratio which is in agreement with 1.75 calculated from Hall measurements taking into account 2.7 $\times$ 10^{19} cm^{-3} electrons induced by oxygen vacancies. The electron Hall mobility is systematically higher for stoichiometric films and decreased due to lattice imperfections and/or secondary phases on top of the films. While doping with La in general decreases resistivity and increases the mobility of the charge carriers, reaching 1.67 cm^2/V s for stoichiometric $E_{0.95}La_{0.05}TiO_{3-\delta}$, Fig. 5.

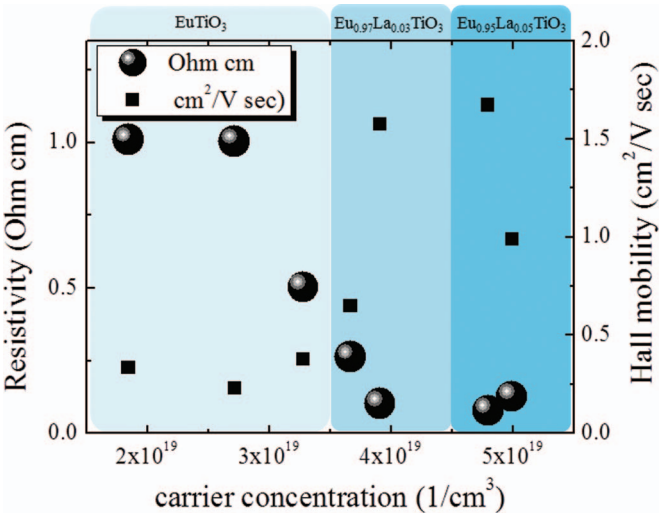

FIG. 5. Room temperature resistivity (left) and Hall mobility (right) obtained for all the samples as a function of electron carrier concentration.

In conclusion, the PLD process of $Eu_{1-x}La_xTiO_{3-\delta}$(x = 0;0.3;0.5) homoepitaxy was studied by controlling the ablation laser energy. The laser fluence was found to have a significant influence on the following:

(i) out-of-plane lattice constant *c*, when independent of La content both Eu^{3+}-rich and Ti^{4+}-rich films exhibit 1% *c*-axis elongation;
(ii) the surface morphology and defect structure, which results in a 1–2 u.c. height terraces (as for as prepared LSAT [001] substrate) for stoichiometric films and the presence of nanorods and round-shape islands for Eu-rich and Ti-rich films, respectively;
(iii) resistivity of the deposited films, which is lowest for stoichiometric films and highest for Eu-rich films within every series except for undoped ETO;
(iv) electron Hall mobility, which is increased for stoichiometric films and consequently increased by doping with higher amount of La.

We thank C. Makovicka for the preparation of the PLD targets and S. Wicklein for technical assistance.

[1] K. S. Takahashi, M. Onoda, M. Kawasaki, N. Nagaosa, and Y. Tokura, Phys. Rev. Lett. **103**, 057204 (2009).
[2] L. Sagarna, A. Shkabko, S. Populoh, L. Karvonen, and A. Weidenkaff, Appl. Phys. Lett. **101**, 033908 (2012).
[3] H. Ohta, S. Kim, Y. Mune, T. Mizoguchi, K. Nomura, S. Ohta, T. Nomura, Y. Nakanishi, Y. Ikuhara, M. Hirano, H. Hosono, and K. Koumoto, Nat. Mater. **6**, 129 (2007).
[4] A. Fujimori, J. Phys. Chem. Sol. **53**, 1595 (1992).
[5] J. Son, P. Moetakef, B. Jalan, O. Bierwagen, N. J. Wright, R. Engel-Herbert, and S. Stemmer, Nat. Mater. **9**, 482 (2010).
[6] G. Rijnders and D. H. A. Blank, Nat. Mater. **7**, 270 (2008).
[7] F. Schoofs, T. Fix, A. S. Kalabukhov, D. Winkler, Y. Boikov, I. Serenkov, V. Sakharov, T. Claeson, L. MacManus-Driscoll, and M. G. Blamire, J. Phys.: Condens. Matter **23**, 305002 (2011).
[8] D. J. Keeble, S. Wicklein, R. Dittmann, L. Ravelli, R. A. Mackie, and W. Egger, Phys. Rev. Lett. **105**, 226102 (2010).
[9] C. J. Fennie and K. M. Rabe, Phys. Rev. Lett. **97**, 267602 (2006).
[10] J. W. Kim, P. Thompson, S. Brown, P. S. Normile, J. A. Schlueter, A. Shkabko, A. Weidenkaff, and P. J. Ryan, Phys. Rev. Lett. **110**, 027201 (2013).
[11] A. P. Petrovic, Y. Kato, S. S. Sunku, T. Ito, P. Sengupta, L. Spalek, M. Shimuta, T. Katsufuji, C. D. Batista, S. S. Saxena, and C. Panagopoulos, Phys. Rev. B: Condens. Matter **87**, 064103 (2013).
[12] J. Cao and J. Wu, Mater. Sci. Eng. R **71**, 35 (2011).
[13] J. H. Lee, L. Fang, E. Vlahos, X. Ke, Y. W. Jung, L. F. Kourkoutis, J. W. Kim, P. J. Ryan, T. Heeg, M. Roeckerath, V. Goian, M. Bernhagen, R. Uecker, P. C. Hammel, K. M. Rabe, S. Kamba, J. Schubert, J. W. Freeland, D. A. Muller, C. J. Fennie, P. Schiffer, V. Gopalan, E. Johnston-Halperin, and D. G. Schlom, Nature (London) **466**, 954 (2010).
[14] K. Tanaka, K. Fujita, Y. Maruyama, Y. Kususe, H. Murakami, H. Akamatsu, Y. Zong, and S. Murai, J. Mater. Res. **28**, 1031 (2013).

[15] A. N. Morozovska, M. D. Glinchuk, R. K. Behera, B. Zaulychny, C. S. Deo, and E. A. Eliseev, Phys. Rev. B: Condens. Matter **84**, 205403 (2011).
[16] R. Ranjan, H. S. Nabi, and R. Pentcheva, J. Appl. Phys. **105**, 053905 (2009).
[17] S. A. Chambers, Surf. Sci. **605**, 1133 (2011).
[18] S. Ohta, T. Nomura, H. Ohta, and K. Koumoto, J. Appl. Phys. **97**, 034106 (2005).
[19] T. Ohnishi, K. Takahashi, M. Nakamura, M. Kawasaki, M. Yoshimoto, and H. Koinuma, Appl. Phys. Lett. **74**, 2531 (1999).
[20] P. Brinks, W. Siemons, J. E. Kleibeuker, G. Koster, G. Rijnders, and M. Huijben, Appl. Phys. Lett. **98**, 242904 (2011).
[21] B. Jalan, R. Engel-Herbert, N. J. Wright, and S. Stemmer, J. Vac. Sci. Technol. A **27**, 461 (2009).
[22] S. Wicklein, A. Sambri, S. Amoruso, X. Wang, R. Bruzzese, A. Koehl, and R. Dittmann, Appl. Phys. Lett. **101**, 131601 (2012).
[23] C. Caspers, M. Mueller, A. X. Gray, A. M. Kaiser, A. Gloskovskii, C. S. Fadley, W. Drube, and C. M. Schneider, Phys. Status Solidi (RRL) **5**, 441 (2011).
[24] C. Gerth, A. Kochur, M. Groen, T. Luhmann, M. Richter, and P. Zimmermann, Phys. Rev. A: At. Mol. Opt. Phys. **57**, 3523 (1998).
[25] W. Schneider, C. Laubschat, I. Nowik, and G. Kaindl, Phys. Rev. B **24**, 5422 (1981).
[26] D. J. Keeble, S. Wicklein, L. Jin, C. L. Jia, W. Egger, and R. Dittmann, Phys. Rev. B: Condens. Matter **87**, 195409 (2013).
[27] A. H. G. Princen, Master thesis, University of Twente, 2007.
[28] H. Kiessig, Ann. Phys. (Berlin) **402**, 769 (1931).
[29] T. Ohnishi, M. Lippmaa, T. Yamamoto, S. Meguro, and H. Koinuma, Appl. Phys. Lett. **87**, 241919 (2005).